Journal of Pharmaceutical Analysis 12 (2022) 164–177

Contents lists available at ScienceDirect

Journal of Pharmaceutical Analysis

journal homepage: www.elsevier.com/locate/jpa

Original article

Biological analysis of an innovative biodegradable antibiotic eluting bioactive glass/gypsum composite bone cement for treating experimental chronic MRSA osteomyelitis

Surajit Mistry [a, *], Subhasish Burman [b], Subhasis Roy [c], Nilendu Jyoti Maitra [d], Rajiv Roy [e], Abhijit Chanda [f]

[a] Department of Periodontics, Burdwan Dental College & Hospital, Burdwan, 713101, India
[b] Department of Oral & Maxillofacial Surgery, Burdwan Dental College & Hospital, Burdwan, 713101, India
[c] Department of Veterinary Clinical Complex (Surgery & Radiology), West Bengal University of Animal & Fishery Sciences, Kolkata, 700037, India
[d] Directorate of Research Extension & Farms, West Bengal University of Animal & Fishery Sciences, Kolkata, 700037, India
[e] Department of Orthopaedics, Calcutta National Medical College & Hospital, Kolkata, 700014, India
[f] School of Bio-Science & Engineering, Jadavpur University, Kolkata, 734432, India

ARTICLE INFO

Article history:
Received 29 June 2020
Received in revised form
18 February 2021
Accepted 25 February 2021
Available online 3 March 2021

Keywords:
Antibiotics
Biodegradable composite
Osteomyelitis
MRSA strains
Osteoconduction

ABSTRACT

A multi-barrier antibiotics loaded biodegradable composite bone cement for resolving chronic osteomyelitis has been studied to understand the physico-mechanical properties, drug loading/eluting efficiency, and different merits and demerits prior to clinical application. After successful induction of bone infection in 28 rabbits using methicillin-resistant *Staphylococcus aureus* (MRSA) strains, calcium sulfate/bioactive glass based composite cement was implanted in 12 defects to assess its performance over parenteral therapy with microscopic and radiological examination for 90 days. The composite cement revealed acceptable physico-mechanical properties and controlled drug elution kinetics. Furthermore, the antibiotics concentrations in bone up to 42 days were sufficient to kill MRSA without eliciting adverse drug reactions. The striking feature of platelets aggregation by composite cement could assist bone healing. The controlled degradation with simultaneous entrapment of composite cement within the osteoid tissues and complete repair of infected cortical defects (holes) in rabbit tibia at 6 weeks indicated the excellent anti-infective and osteoconductive properties of composite cement. Thus, the animal study demonstrated the superiority of composite over injectable antibiotic therapy based on infection resolution and bone regeneration. We thereby conclude that the composite cement can be effectively applied in the treatment of resistant cases of chronic osteomyelitis.

1. Introduction

Nowadays, the incidence of chronic osteomyelitis has drastically increased due to the increased number of road traffic accidents, injuries and widespread use of prosthesis in orthopaedics. The chronic bone infection is difficult to treat with a characteristic feature of frequent relapses despite combined medical and surgical therapies. The mainstay treatment protocols of chronic osteomyelitis are surgical removal of necrotic tissues, copious saline irrigation, management of dead space, proper wound margin approximation, and a long-course regimen (4–6 weeks) of antibiotics [1]. The conventional routes of antibiotic therapy following surgical debridement of necrotic tissues are ineffective in eradicating chronic osteomyelitis because of the limited entry of drugs in the avascular bone (sequestrum) and biofilm forming habit of the culprit organisms, i.e., commonly methicillin-resistant *Staphylococcus aureus* (MRSA). An adequate concentration of antibiotics, about 1000 times more than the minimal inhibitory concentration (MIC), for extended period can hardly be attained by the traditional routes of delivery to destroy the biofilm bacteria at local sites

Peer review under responsibility of Xi'an Jiaotong University.
* Corresponding author.
E-mail address: dr.surajitmistry@rediffmail.com (S. Mistry).

https://doi.org/10.1016/j.jpha.2021.02.005

without causing serious side effects, which thus, increases the relapse rate [1]. Since polymethyl methacrylate (PMMA) is porous and groutable, it has been widely examined as local drug delivery system (LDDS) or bone cement and found to be effective for antibiotic delivery in osteomyelitis [1]. However, PMMA discloses several limitations as LDDS including sub-optimal release, thermal damage to tissue/antibiotics, and surgical re-entry for cement removal [2,3]. Therefore, scientific focus has been directed toward biodegradable carriers that deliver sufficient antibiotics at the site of infection, facilitate osteogenesis, and obviate the need for bead removal surgery. Several biodegradable materials, namely, calcium phosphates, calcium sulfate hemihydrate (CSH), bioactive glass (BG), synthetic polymers and composites, have been used as LDDS [4–7]. The major shortcomings of highly porous CSH cement (i.e., poor strength and osteogenicity and quick drug elution kinetics) have been partially rectified by converting the β-CSH to stronger and denser α-CSH crystals or combining α-CSH with other bioceramics and polymers [4,7]. The BG scaffold has been proven to be effective as an LDDS and its degradation rate closely matches the ossification rate [6]. Nowadays, synthetic poly lactide-co-glycolide (PLGA) has gained high priority as LDDS, because it exhibits cell adhesion property, intercepts 'burst elution' of drugs and improves strength and flow characteristics of the coated constructs [8,9]. A combination of antibiotics in bone infection is preferred for synergistic bactericidal action against all the causative organisms of osteomyelitis and to reduce the bacterial resistance and toxicity of the individual drug [10]. Vancomycin hydrochloride (V_H) and tobramycin sulfate (T_S) antibiotics are hydrophilic, thermo-stable, and show passive opportunism; hence, the combination is suitable for loading in bone cements [11,12]. The size, volume, distribution, and relation of open porosity of the scaffolds may have an important role in drug adsorption/elution behavior and bone formation. The macropores (>50 μm) permit osteoblast infiltration into the scaffolds, and micropores (<10 μm) and mesopores (10–50 μm) are essential in preventing 'burst release' of antibiotics [5]. However, the scaffolds in a pellet form are hard enough to apply in isolated areas of bone. Therefore, the biodegradable composite cement has been tried as a convenient alternative to the prefabricated scaffolds that can favor ease of application in adjunct to acceptable drug delivery. A majority of the CSH-BG composite bone cements available in literature are prepared by mixing of CSH and BG in powder form with other biomaterials (i.e., chitosan, cellulose, polymers, etc.) for infection control and bone regeneration purpose [4,7,13]. According to our understanding, no effort has been devoted hitherto to preparing composite bone cement by encapsulating the antibiotics incorporated porous BG granules with PLGA and α-CSH. Our hypothesis is that the coating of antibiotic filled porous BG granules by PLGA and α-CSH can provide a multi-barrier effect on drug release in addition to rapid bone healing because of the high osteogenic potential of BG crystals [3,6,7]. Furthermore, the influence of PLGA coating and antibiotic on the mechanical property of new cement has yet to be explored. In this study, we reported the development of a biodegradable α-CSH/BG bone cement and examined its physico-mechanical properties and tailoring ability in releasing loaded antibiotics (i.e, V_H/T_S), as well as outlining its performance in eradicating chronic MRSA osteomyelitis in contrast to conventional antibiotic treatment in rabbit tibia.

2. Materials and methods

2.1. Process of pure α-calcium sulfate hemihydrate preparation

Calcium sulfate dihydrate (CSD) cake was produced via hydration of β-CSH powder (Merck, Mumbai, India) with normal saline and kept in saturated humidity for 7 days. The dried CSD powder (37 °C) was soaked into aqueous solution of sodium succinate (0.15%, *m*/*V*) to coat the CSD particles with crystal habit modifier and dried overnight. The powder mass was then autoclaved at 130 ± 5 °C under 40 ± 5 psi saturated vapor state for 3 h and then oven dried (105 °C) for 8 h. The calcined product was powdered in a ceramic ball grinding mill for 4 h, and then filtered out the organic impurities after acetone rinse using vacuum. The fresh powder (1 kg) was mixed with each 20 g of potassium sulfate and CSD powder and sieved twice using British standard sieve # 200 (BSS, <75 μm) to obtain the desired particle size (Supplementary data).

2.2. Process of porous bioactive glass granules preparation

As shown in the Supplementary data, the BG was synthesized by conventional glass melting procedure (1400 °C) from a mixture of network modifiers and glass former including silica (43%–44%), decahydrated borax (6%–7%), sodium carbonate (11%–12%), calcium carbonate (29%–30%), di-ammonium hydrogen orthophosphate (8%–9%), and 1%–2% titanium oxide (all analytical reagent grade chemicals, S D Fine-Chem Ltd., Chennai, India). The detailed method of processing and in vitro characterization has been reported earlier [14]. The final chemical composition of this glass obtained with inductively coupled plasma-atomic emission spectral study (Spectro Analytical Instruments, Spectroflame Modula, Kleve, Germany) was found to be about 43.72% SiO_2, 19.2% CaO, 5.46% P_2O_5, 9.38% B_2O_3, and 22.24% Na_2O, which has been used for fabrication of granules. The BG powders and porogen β-naphthalene (S D Fine-Chem Ltd., Chennai, India) were pulverized in ball mill and sieved (BSS# 50) separately. The BG and β-naphthalene powders (40:60 *m*/*m*, respectively) were mixed uniformly by sieving (BSS # 50) thrice in an automatic shaking device and then cold iso-pressed (EPSI NV, SO 10036, Temse, Belgium) at 150 MPa (1 min) to make barrel-shaped rods. Next, the machined discs (thickness about 1 cm) were placed over platinum crucible lid and thermally treated in a dryer from room temperature (RT) to 80 °C for 8 days. By the slow and incremental heating, the naphthalene was vaporized entirely from the discs without cracking at this stage. Finally, the lid containing frail discs were sintered at 690 °C for 8 min using a dental laboratory oven (Vita Vacumat 40T, Bad Säckingen, Germany) in air. Then, the discs were carefully crushed with a pestle and agate mortar and then sieved between BSS# 30–50 in the sieve shaker to obtain BG granules.

2.3. Characterization of prepared products

Compositional natures of the β/α-CSH and BG powders were assessed by X-ray diffraction (XRD) analysis (X'pert PRO, Phillips Analytical B.V., Almelo, the Netherlands) (Fig. S1) and Fourier-transformed infra-red (FTIR) spectroscopy (Spectrum™ 100, PerkinElmer, Waltham, MA, USA). Zeta potential (Microtrac FLEX 10.6.1 software, Zetatrac, Haan, Germany) of the powders at different pH state (pH 4.5–8.4) was measured for indirect estimation of electrostatic interaction between the component molecules. The differential scanning calorimetry (DSC, STA 449F1, Jupiter®, NETZSCH, Selb, Germany) analysis was conducted to verify the transformation of β-CSH phase. The powder morphology was examined under field-emission scanning electron microscope (Sigma VP, Carl Zeiss, Oberkochen, Germany) equipped with energy dispersive X-ray (FESEM-EDX) analysis. Subsequently, the pore characteristics and morphology of BG globules were assessed by 2D-image analysis software (Leica Q500MC, Cambridge, UK). Mercury porosimeter (PM60, Quantachrome Poremaster 7.01, Quantachrome Corp., Boynton Beach, FL, USA) was used to measure the open pores (*V*%), distribution of pore size, and density of the porous BG granules by volume-intrusion method.

2.4. Antibiotics incorporated composite bone cement preparation

An appropriate amount of BG granules was immersed separately in the aqueous solution of V_H (200 mg/mL, Cipla, Mumbai, India) and T_S (160 mg/mL, Livzon NNR Pharma Co., Ltd., Qingyuan, Guangdong, China). The drugs were vacuum infiltrated (10^{-3} Torr for 2 h) into the porous ceramics and then completely dehydrated in a freeze drier under vacuum for 8 h. The vancomycin and tobramycin loaded BG (VBG and TBG, respectively) samples were collected from the beaker and weighed to assess for sorption capacity of BG granules in percentage $((W_2-W_1)/W_1 \times 100$, where W_1 is the weight of BG, and W_2 is the weight of drug loaded BG granules). The agglomerate free VBG and TBG granules were stirred manually in 2% (*m*/*V*) PLGA (lactide:glycolide 75:25 (*V*/*V*), Sigma Aldrich, St. Louis, MO, USA), mixed with acetone solution and exposed to 25 Torr vacuum (30 s) for better encapsulation of PLGA layer on BG granules. The samples were spread repeatedly on a glass slab with a non-sticky spatula until total disappearance of acetone at RT to avoid the fusion of coated particles. Finally, the BG/CSH bone cement (α-CSBG) powder was prepared by mixing 65% α-CSH powder with 15% polymer (PLGA) coated VBG and 20% PLGA coated TBG granules (Table 1). About 1 g of powder was loaded in each double-covered container prior to γ ray sterilization. Vancomycin powder (additive) was mingled with the composite powder before mixing with sterile water dropwise for the preparation of vancomycin mixed α-calcium sulfate-bioactive glass cement (α-CSBGV) beads. The β-CSBGV and additive free α-CSBG beads (1 g) were also prepared for research inquiries (Table 1). Liquid to cement powder (l:p) ratio was 0.45–0.8 mL/g. Furthermore, the control beads were prepared by mixing defined amounts of VBG and TBG with α-CSH powder in absence of additive to examine the tailoring ability of PLGA on drug release. The composite cements were set by mild exothermic hydration reaction. After mixing with water, the water of crystallization of α-CSH ($0.5H_2O$) was increased and finally converted into the hard mass of interlocked needle-like crystals network of CSD ($2H_2O$), embracing the BG granules.

2.5. Characterization of bone cement specimens

The FTIR spectroscopy was again performed for PLGA coated granules and α-CSBG powders, and set constructs to identify the change in composition, if any, after γ ray sterilization and exothermic setting reaction. The carbon coated samples were examined under FESEM-EDX to check the antibiotic uptake zones and characteristics of PLGA coating.

2.6. Physico-mechanical properties of cement

2.6.1. Setting time and setting temperature

Initial setting time (IT) of the cements using 2.12 mm diameter Gillmore needle and final time (FT) with 1.06 mm needle were computed at (27 ± 1) °C and (20 ± 1) °C, in triplicate, according to a procedure stated previously [15]. Setting temperature was recorded with a thermometer.

Table 1
Weight percentage (%) of components in bone cements.

Cement parts	Contents	α-CSBG	β-CSBG
Powder (%)	CSH (α/β)	65 (α)	65 (β)
	PLGA-VBG	15	15
	PLGA-TBG	20	20
Additive (%)	V_H/T_S	5 V_H	5 V_H
Liquid		Water/NS	Water/NS
Liquid:powder ratio	Thick mix	0.45 mL/g	0.7 mL/g
	Injectable	0.6 mL/g	0.8 mL/g

CSBG: calcium sulfate-bioactive glass; V_H: vancomycin; T_S: tobramycin; PLGA: poly lactide-co-glycolide; VBG: vancomycin loaded bioactive glass; NS: normal saline; TBG: tobramycin loaded bioactive glass.

2.6.2. Compressive strength

The compression failure load of β/α-CSH and cement cylinders (size: 8 mm × 16 mm) was recorded by Universal Testing Machine (UTM, Instron 5500R, Canton, High Wycombe, Bucks, UK), in triplicate, according to the ASTM C773 standard at constant rate of 1 mm/min crosshead displacement [15].

2.6.3. Porosity of set constructs

The dehydrated cylinders of β/α-CSBG were submerged in distilled water for 30 min, gently mopped with tissue paper, and weight gain was calculated to determine the percentage of open porosity by water immersion technique using Archimedes' principles $((W_f - W_i)/W_i \times 100$, where W_f is the wet weight and W_i is the dry weight of β/α-CSBG cylinders). The bulk density of set specimens was measured by dividing the dry weight (W_i) by the volume of cylinders.

2.6.4. Injectability

About 3.5 mL of cement pastes (working time: 45 s) was injected through 5 mL needleless plastic syringe (internal diameter: 1.3 cm, nozzle diameter: 0.3 cm, piston surface area: 1.33 cm^2, idle period: 30 s) and extrusion load was measured (piston shift: 15 mm, speed: 15 mm/min) using the UTM machine. The injectability was taken to mean the amount of paste ejected from the nozzle and dividing the value by weight of the total in percentage [15].

2.7. In vitro antibiotics release studies and pH test

The amount of V_H and T_S was about 33 mg and 28 mg in α-CSBG and control beads, and 83 mg and 28 mg in α-CSBGV beads, respectively. The set cylinders (1 ± 0.05 g) of α-CSBG, α-CSBGV and control cements were submerged in 3 mL of simulated body fluid (SBF; pH 7.4) and fresh human plasma (FP) separately at 37 °C. The total solutions were removed from the test tube at specified intervals and stored at −80 °C. The beads were restored with an identical volume of liquid after gentle rinse and incubated again. The FP carrying tubes were gently shaken for 1 min prior to incubation for liquefaction of fibrin clot around the beads. The standard for plasma samples was prepared by spiking blank FP with the stock solution prepared in distilled water. The pH value of the SBF after recovery from α-CSBG container was recorded using a pH meter.

The V_H in elutes was quantified using high performance liquid chromatograph (HPLC, Metrohm Ltd., Herisau, Switzerland), fitted with UV–vis Bischoff lamda 1010 detector, and RPC_{18} (150 mm × 4.6 mm i.d., 5 μm) XBridge® column (Waters, Dublin, Ireland). The mobile phase was composed of acetonitrile (10%) in 0.025 M phosphate buffer (3.402 g of KH_2PO_4 added in 1 L of HPLC grade water and HCl was used to adjust pH at 7.0). The mobile phase flow rate was of 1 mL/min and V_H was detected at wavelength of 214 nm with retention time of 9.4 min. After filtration, 10 μL of SBF sample was infused into the HPLC system. The V_H was extracted by depoteination of 1 mL of standard or test FP sample with 50 μL of 70% perchloric acid in the microcentrifuge tubes [16]. The samples were vortexed (1 min) and centrifuged at 10,000 r/min for 10 min to settle down the blood proteins. The superficial fluid was collected and filtered in 0.22 μm membrane filter before injecting (10 μL) into the system. The chromatograph value of V_H in FP was adjusted manually to obtain the real concentration by eliminating the dilution factor.

The concentration of T_S was measured by well diffusion bioassay method [17] inoculating *Escherichia coli* on Mueller-Hinton (MH)

agar medium (Himedia, Mumbai, India). About 0.2 mL of the cell suspension (0.5 McFarland standard) was evenly spread on the agar plates with a sterile cotton swab. Next, 20 μL of triplicate samples were pipetted into the wells (8/plate). The agar plates were restored at (35 ± 0.02) °C for 20 h and zones of inhibition were measured using a caliper within 0.1 mm. The quantity of eluted T_S for each interval was calculated with reference to a linear standard curve of 2.5–100 μg/mL. The rate of drug release was calculated through dividing the eluted amount by the incorporated amount in percentage.

2.8. Indirect biodegradability, bioactivity and cytocompatibility test

The cylinders were recovered from SBF after 6 weeks of drug release test and dried overnight at 55 °C. The biodegradability (W_d) of the samples was calculated by dividing the difference in specimen weight from pre- to post-drug elution by the pre-elution weight (adjusting drug amount) in percentage (W_d (%) = (W_a − W_b)/W_a × 100, where W_a is the weight of the beads before drug elution and W_b is the weight after drug elution). The specimens were further studied using FTIR and SEM-EDX to ascertain the precipitation of apatite crystals on the bead surfaces.

The cytocompatibility of the α-CSH and α-CSBG composite beads (dimension: 8 mm × 3 mm) was assessed with 3-(4,5-dimethylthiazol-2-yl)-2,5-diphenyl tetrazolium bromide (MTT) assay method [7] using mouse osteoblast precursor cells (MC3T3) within 24-well cell culture plates. The cell aggregates were grown to subconfluent layers in alpha minimum essential medium (α-MEM, GIBCO®, Thermofisher Scientific Inc., Waltham, MA, USA) containing fetal bovine serum (10%) and streptomycin (100 mg/L, Sigma Aldrich, St. Louis, MO, USA) solution and preserved in the incubator (ESCO Pte Ltd., Singapore) with 5% CO_2 and 95% humidity at 37 °C. Cell clusters were placed onto the sterile samples (1×10^4 cells/sample) and 1 mL of α-MEM solution was added. The plates were incubated in an atmosphere of 5% CO_2 in moist air at 37 °C. Growth media were replaced every other day. After the samples were incubated for 1, 3, and 7 days, the medium was removed and each sample was washed thrice with phosphate-buffered saline (PBS). Then, 200 μL of MTT solution (5 mg/mL in PBS) was pipetted into each well. After incubation for 4 h in the moist CO_2 atmosphere at 37 °C, MTT medium was cautiously removed. Next, 500 μL of dimethyl sulfoxide (Sigma Aldrich, St. Louis, MO, USA) was added to solubilize and extract the insoluble purple formazan salts. Finally, the assay liquids were shifted to 96-well plates and the absorbance (optical density) of the wells was quantified with a plate reader (Bio-Rad Instrument, Hercules, CA, USA) at 595 nm. The cells-attached beads were taken out from the plates and fixed for 24 h with 2% glutaraldehyde solution at 4 °C. The dehydration of cells was done by treating the samples with ethanol series (30%, 50%, 70%, 95%, and 100%) and by ethanol-hexamethyldisilazane (HMDS, CAS No. 999-97-3, Alfa Aesar, Haverhill, MA, USA) series for 10 min, and finally, by 100% HMDS overnight. The gold sputtered samples were observed under SEM to assess the cell morphology and pattern of growth on the samples. The cell proliferation on α-CSBG beads was compared with that on α-CSH beads using independent sample *t*-test on MTT assay data.

2.9. Preparation of bacterial suspension

The coagulase-positive MRSA germs were acquired from a known case of chronic osteomyelitis (as per swab culture) and grown on MH plate at 37 °C. At least 2–3 isolated colonies were diluted with normal saline to obtain the turbidity equivalent to 0.5 McFarland standard (1×10^8 CFU/mL) and the cell suspension was used for the induction of osteomyelitis in rabbits.

2.10. In vivo experimentation

2.10.1. Animal research

The Ethics Committee for Animal Research of the Ram Krishna Ashram Krishi Vigyan Kendra, Nimpith, South 24-Parganas, West Bengal, India, approved the study protocol in accordance with the guidelines of the Committee for the Purpose of Control and Supervision of Experiments on Animals (CPCSEA, India). The proximal end of the left tibia of 28 white New Zealand rabbits (2–2.5 kg) were exposed after general anaesthesia with xylazine hydrochloride 20 mg/kg (Xylo-B, Brilliant Bio-Pharma., Hyderabad, India) via intramuscular route. A borehole was created through cortical bone using dental micromotor fitted with 1 mm diameter dental bur. About 0.2 mL of suspension (2×10^7 CFU MRSA) was injected into the marrow cavity and the orifice was sealed with bone wax to avert soft tissue infection. The animals were watched carefully after closure of wounds. Intramuscular ketoprofen (3 mg/kg body weight for 2 days) was administered for pain relief. After 4 weeks, swab specimens (pus) were collected from the wounds and incubated in an overnight culture of 1% peptone water to verify the development of infection using Gram's staining technique. According to the treatment plan, the diseased animals were distributed randomly into two groups: Group I (parenteral antibiotics group) and Group II (α-CSBGV). The details of the research plan for animal trial are shown in Table 2. The development of osteomyelitis was confirmed with four animals euthanized randomly (2/group) after 28 days of stage 1 surgery by microbiological test (MT) and histopathological examination (HPE), and by radiographs for all animals. On the 35th day, the defects were re-entered (stage 2 surgery) and enlarged up to 4–5 mm by dental drill. After thorough debridement of marrow cavity with a sterile spiral wire, the tissue samples were collected from all the animals to verify the presence of bone infection with MT and HPE. Then, 0.75 g of α-CSBGV was impacted in and around each toileted wound of 12 animals. After surgical debridement, intramuscular V_H and T_S twice daily for 42 days were given to the remaining 12 animals without applying bone cements into the defects. The wounds were sutured and post-operative analgesic was re-instituted for 3 days.

2.10.2. Post-operative assessment

The sedated animals (3/group) were euthanized medically on 14, 28, 42, and 90 days after stage 2 surgery (post-implantation, p.i.) to distinguish the effect of two therapeutic approaches by evaluating the MT, HPE, radiograph, SEM, and drug levels in plasma and bone. The histological sections (3 slides/animal × 3 = 9 sections/group/interval) were interpreted digitally by degenerative (bone/myeloid damage), inflammatory (number of inflammatory cells, pus), resorptive and reparative (osteoid formation, growing mesenchyme) features; scored from 0 to 3 (score '0': absent, '1': scanty/mild, '2': moderate, and '3': abundant/marked, where high score indicated the poor healing and reparative features earned '-ve' score). The radiograph of the defects was captured (Genius 100, GE Healthcare, Hyderabad, India) to observe the cement beads and changes around the defects. The dried bone (ethanol/acetone) samples were studied using back-scatter mode of SEM (Phenom proX, Phenom-World B.V., Eindhoven, the Netherlands) and cellular events were graded following the aforesaid criteria. The blood from marginal ear vein and supernatant of crushed cortico-cancellous bone mixed SBF were retrieved after centrifugation for assessment of antibiotic concentrations.

2.11. Analysis of statistical data

The data of compressive strength, cell culture, HP score, and SEM score were analyzed using IBM SPSS (version 21, SPSS Inc.,

Table 2
Research plan for animal experimentation.

Group	Lot of rabbits	Treatment given	Time of examination	Investigation and animals euthanized (3 animals/interval after stage 2)
Stage-1 surgery	28	No (infection induced)	At 4 weeks: 2 groups assigned	Two animals/group euthanized for X-Ray, MT, HPE, and SEM to justify the occurrence of osteomyelitis.
Group I (Stage-2)	12	SD + injection V_H (40 mg/kg, b.i.d.) and T_S (2.5 mg/kg, t.i.d.) i.m. for 6 weeks	14, 28, 42 days p.i.	- MT, HPE, X-ray, SEM, and DC in plasma/bone
			90 days p.i.	- MT, HPE, X-ray, and SEM.
Group II (Stage-2)	12	SD + α-CSBGV beads	14, 28, 42 days p.i.	- MT, HPE, X-ray, SEM, and DC in plasma/bone
			90 days p.i.	- MT, HPE, X-ray, and SEM.

MT: microbiological test; HPE: histopathological examination; p.i.: post implantation/stage 2; SEM: scanning electron microscopy; SD: surgical debridement; V_H: vancomycin; T_S: tobramycin; i.m.: intramuscular; b.i.d.: bi-daily; t.i.d.: thrice daily; DC: drug concentration; CSBGV: vancomycin mixed calcium sulfate-bioactive glass cement.

Chicago, IL, USA) software program. The significance of mean differences at 5% level ($P<0.05$) was determined between two groups (inter-group) using independent samples *t*-test and within a group (intra-group) using paired *t*-test.

3. Results

3.1. Characterization of prepared samples

The detailed characterization of the powders and BG scaffold has been published earlier [18,19]. In brief, the low intensity XRD peaks (Figs. 1B and C) at 2θ = 14.68°, 25.6°, and 29.72° of β-CSH were shifted and changed to stronger peaks (14.62°, 25.51°, and 29.64°). While peak at 31.64° (204) was notably lower and small CSD peaks (20.6°, 29.3°, and 31.4°) in β-CSH disappeared after curing, which indicated the formation of dense, CSD-free, highly crystalline α-CSH (JCPDS# 43–0605). The peaks for CSD reappeared after hydration. XRD patterns of BG powder and granules showed no sharp peaks (amorphous) and identical hump positions after sintering (Figs. 1A and S1), indicating its desirable properties of effective drug adsorption and resorption in situ.

The FTIR spectra for BG granules showed well-defined bands at 460, 778 and 1048 cm^{-1}, which might be due to Si–O–Si bending, Si–O–Si symmetric stretch, and asymmetric stretch vibration of the bridging oxygen anions within silica tetrahedron, respectively (Fig. 2B). The weak band at 1627 cm^{-1} for molecular water, 1454 cm^{-1} for C–O of CO_3^{2-} group and a broad peak at 3430 cm^{-1} was assigned to silanol (Si–OH) or –OH group. These bands were also shown in α-CSBG with slight peak shift at 458, 761, 1053, and 3436 cm^{-1} respectively due to structural reorientation after incorporation of PLGA, CSH, and antibiotics (Figs. 2B and C). In the

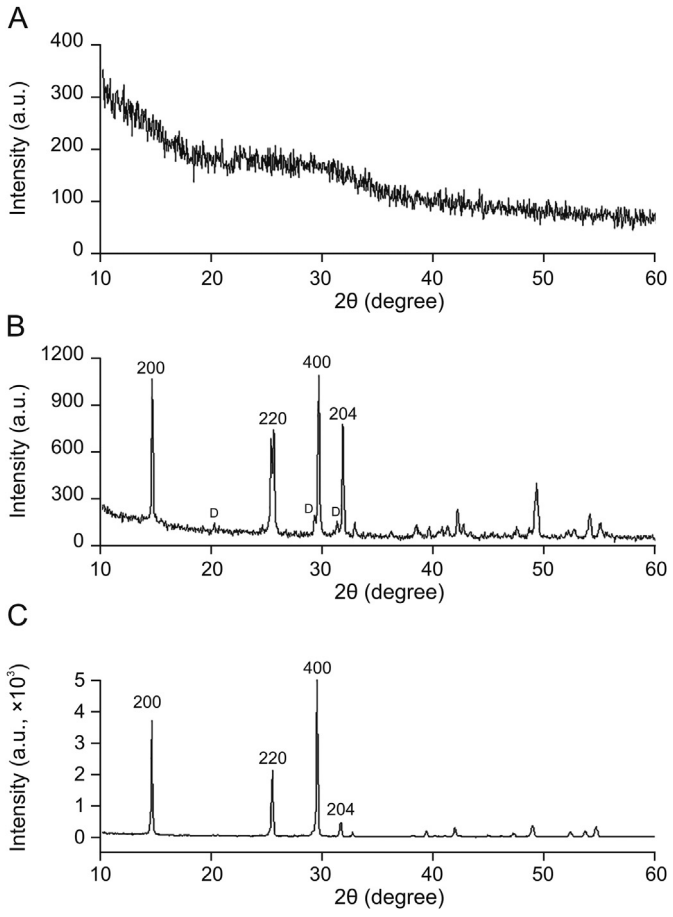

Fig. 1. X-ray diffraction patterns of (A) sintered bioactive glass (BG) granules (690 °C), (B) β-calcium sulfate hemihydrate (β-CSH, #45-0848), and (C) α-CSH particles (# 43-0605). D: dihydrate.

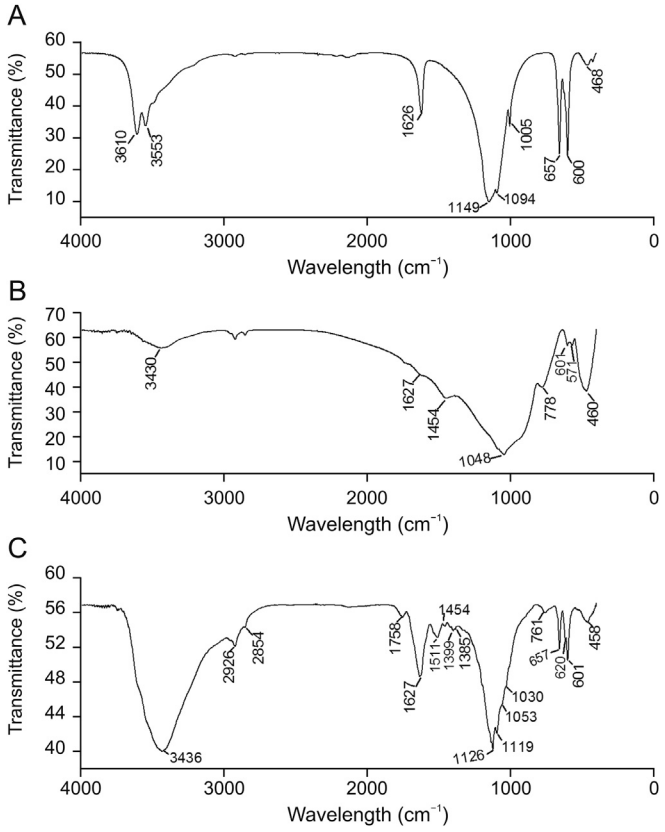

Fig. 2. Fourier-transformed infrared spectra of (A) α-CSH powder, (B) sintered BG granules at 690 °C, and (C) α-calcium sulfate-BG (α-CSBG) bone cement.

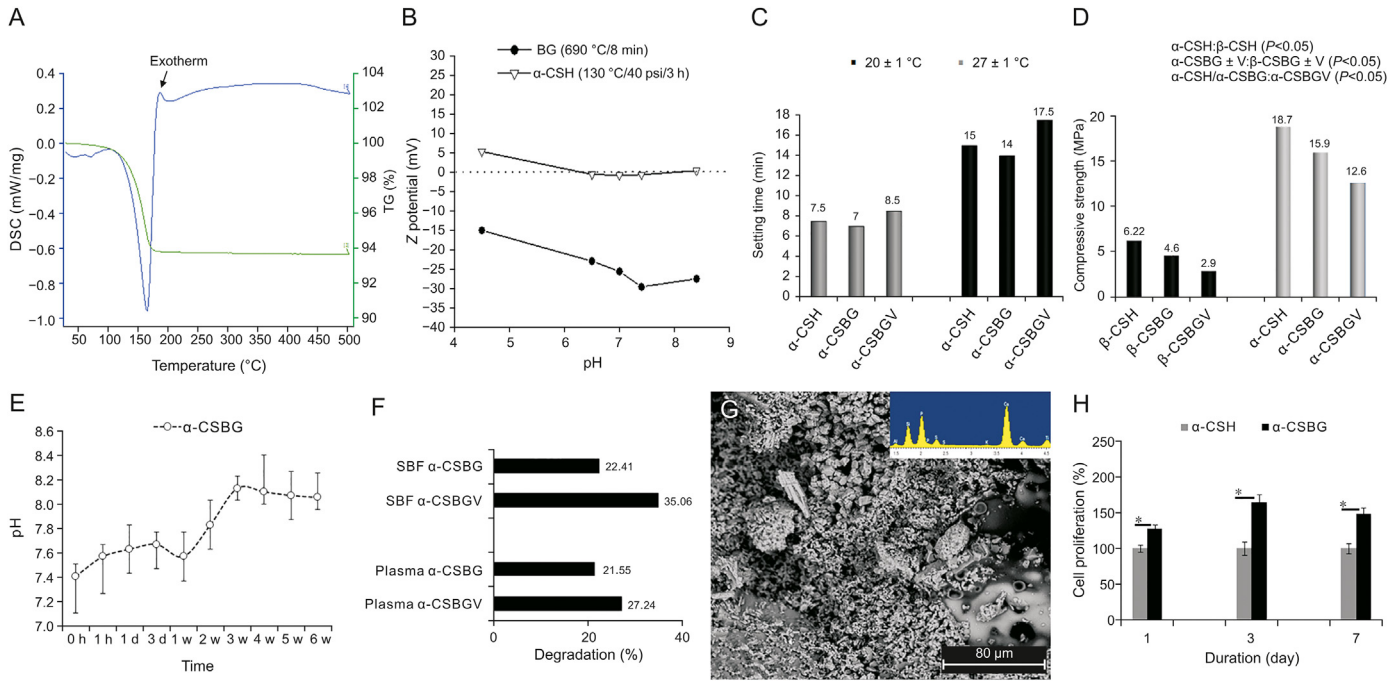

Fig. 3. (A) Differential scanning calorimetry-thermogravimetry (DSC-TG) plot of α-CSH reveals an exotherm (187 °C) after endothermic peak (166 °C), (B) zeta potential for BG and α-CSH powder at variable pH, mean data of (C) final setting time, (D) compressive strength and (E) pH variation of simulated body fluid (SBF), (F) percentage degradation of different beads in plasma and SBF, (G) apatite precipitates on α-CSBG beads after 6 weeks, and (H) MC3T3 cell viability (%) on cement beads with time (*P<0.05, independent t-test). CSBGV: vancomycin mixed calcium sulfate-bioactive glass cement.

γ-ray sterilized α-CSBG cement, FTIR peaks at 1511 (C═C stretching), 1399 (CH_2 deform), and 1126 cm^{-1}(C—N stretch) were attributed to V_H and peaks at 2926 (asymmetric C—H stretch), 1385 (OH bend), 1119 (C—O stretch), and 1030 cm^{-1} (C—N stretch of NH_2) were for T_S (Figs. S2 and S3). The drugs were not destroyed after sterilization. A typical peak of —C═O stretching at 1757 cm^{-1} for PLGA and peaks at 657, 1094, 1626, and 3610 cm^{-1} for α-CSH were invariably found in the cement formulation (Fig. 2A and Supplementary data).

A unique peak for exotherm at 187 °C right after the endothermic peak at 166 °C in DSC curve (Fig. 3A) confirmed the conversion of CSD to α-CSH. The double endothermic peaks (148 °C and 169 °C) and blunt exotherm for CSD (356 °C) and β-CSH (343 °C) were not noticed in the plot (Fig. S4) for α-CSH [19,20]. The thermogravimetry plot showed a drop of 6.21% due to loss of water of crystallization for α-CSH and 19.82% for CSD during anhydrite conversion. The negative surface charge in relation to zeta potential for BG (Fig. 3B) and neutral charge (near iso-electric point) for α-CSH were observed at all the physiologic pH variations (pH 4.5—8.4). In FESEM micrograph, the flat, irregular morphology of CSH crystals (Fig. 4A) was remarkably altered to prismatic (hexagon) bars (length:width = 3:1) along with few small crystals (Fig. 4B) implying total reversal of CHD (Fig. S5) into compact α-CSH particles [20,21]. These changes might improve the strength and workability as well as reduce the resorbability and porosity of the gypsum-based bone cement [21]. The pore structure of BG granules showed three varieties of pores (mostly micro/mesopores and few macropores) with moderate sub-surface interconnection (1—10 μm), and absence of grain boundaries between the particles (Figs. 4C and S5). Average pore size for BG granules was calculated as 31.4 μm and open porosity was about 33.1%. Thick layer of adsorbed drug and uneven thickness of PLGA were observed on the surface of BG granules (Figs. 4D—F, S6, S7). At least 67% ± 3.0% of the outer surface of a BG granule was covered with a thick layer (30—70 μm) and the rest of the surface area with even or interrupted thin layer of polymer (0—30 μm). The bulk density and open porosity of ceramic discs, granules, and set specimens are given in Table 3. The open porosity of BG discs remarkably diminished after conversion of discs into granules, whereas bulk density enhanced. The adsorbability of antibiotics into the granules relied on chemical nature of the drug moieties and open porosity (%) of BG granules. V_H was loaded up to 23% ± 2.0% and T_S was loaded up to 16% ± 3.0% in the BG granules.

3.2. Physico-mechanical properties of cements

3.2.1. Setting time and temperature

Fig. 3C shows the mean FT values of the α-CSBG and α-CSBGV at (27 ± 1) °C and (20 ± 1) °C. The IT of α-CSBG cement at 27 °C was 6.5 min and at 20 °C was 10.5 min. The mixing kit and room temperature variation jointly revealed more profound retardation of setting time (maximum: 9 min) of the cement compared to the use of additive (maximum: 3.5 min) or the mixing methods. The heat energy released during exothermic setting reaction of the cement was around 38 °C.

3.2.2. Compressive strength, porosity, and injectability of cement

The α-CSH based cements were about 3—4 times stronger and had significantly lower (P<0.05) volume of open porosity than the β-CSH composites (Fig. 3D and Table 3). The compressive strength of pure α-CSH (18.7 ± 1.8 MPa) was decreased insignificantly (P>0.05) after mixing of PLGA coated BG granules (15.9 ± 1 MPa). Further, the mixing of V_H additive in the α-CSBG cement reduced the strength markedly (12.6 ± 0.8 MPa, P<0.05). It indicated that both the constituents, especially V_H additive, had a significant negative impact on the strength of cement. About 78.59% ± 1.07% of total weight of α-CSBG paste was injected by (23.77 ± 2.96) N forces.

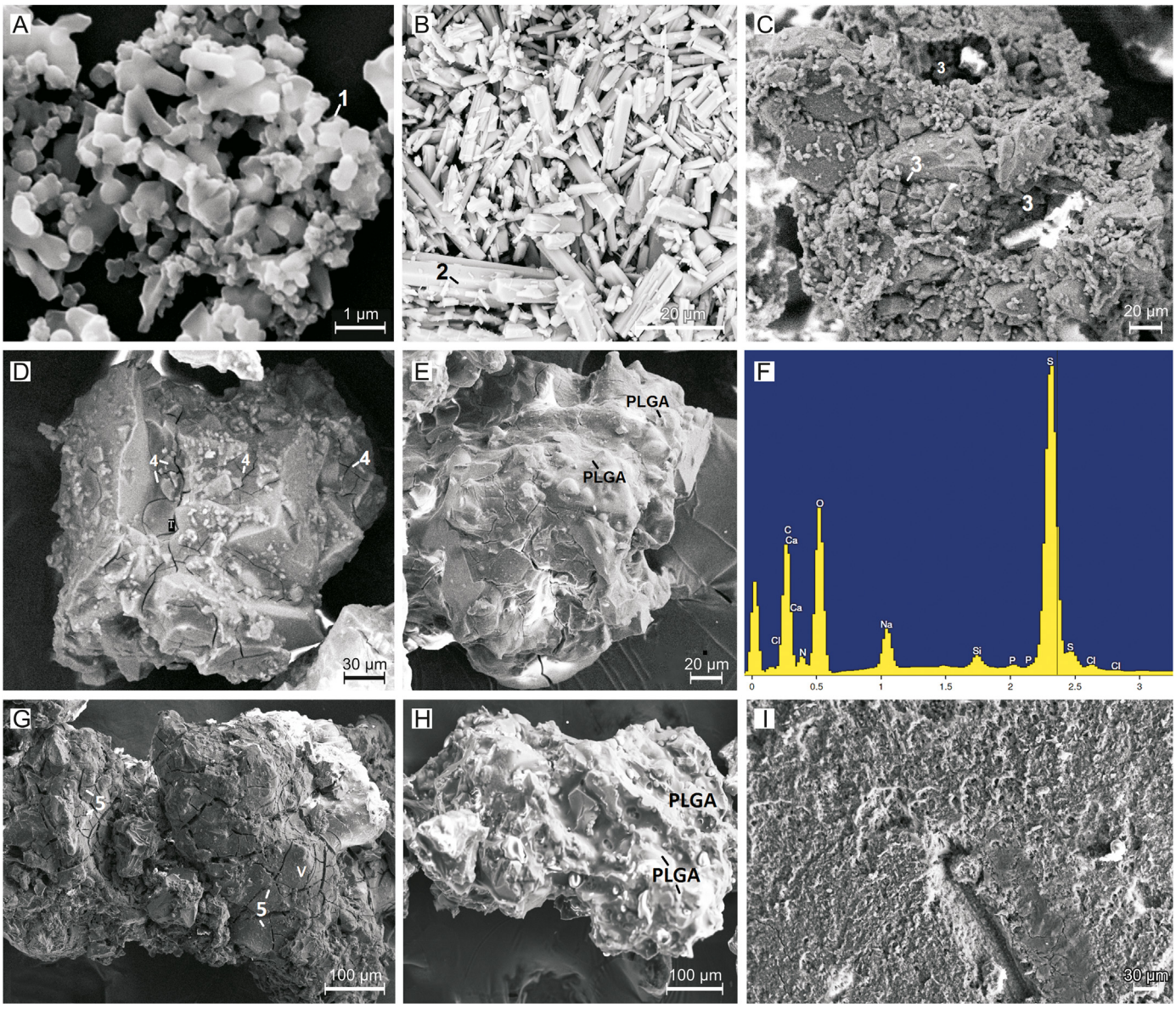

Fig. 4. Scanning electron microscopy micrographs of (A) flat, irregular β-CSH (1), (B) hexagonal α-CSH (2), (C) porous (3) BG granules, (D) tobramycin (T_S, 4) loaded, and (E) poly lactide-co-glycolide (PLGA) coated T_SBG granules, (F) energy dispersive X-ray plot shows drug absorption (C, N, O elements) in BG granules, (G) vancomycin (V_H, 5) loaded, and (H) PLGA coated V_HBG granules, (I) surface of set α-CSBGV.

Table 3
Bulk density and open porosity of BG discs, granules and set cements.

Samples	Bulk density (g/cm^3)	Open pores (*V*%)
BG discs†	0.97 ± 0.05	71.8 ± 1.07
BG granules*	2.01 ± 0.07	33.1 ± 1.5
β-CSBG set cylinder†	0.94 ± 0.04	44.3 ± 1.3
α-CSBG set cylinder†	1.8 ± 0.07	38.4 ± 1.5

† Measured by Archimedes principle; * Mercury Porosimetry test. BG: bioactive glass; CS: calcium sulfate.

3.2.3. *In vitro antibiotics elution*

Elution profile and release percentage (days 1 and 42) of V_H and T_S in SBF and FP for the cement beads are illustrated in Figs. 5A–E, and Tables S1–S5. Both the concentration and amount of 'burst' and sustained mode of V_H release from all the beads in SBF were 50% higher than those in FP, but the elution of T_S was affected minimally. The higher concentrations of drugs were released to a more sustainable mode from the additive carrying α-CSBGV pellets in either elution medium compared to the α-CSBG pellets [11]. The release of T_S from α-CSBG and α-CSBGV pellets was stopped after 21 and 35 days, respectively, in both media. On day 1, the average concentration of V_H released from the uncoated control beads and α-CSBG in FP was 7.5 mg/L (60.1%) and 3.85 mg/L (35%) and T_S was 1.4 mg/L (14.2%) versus 0.96 mg/L (10.3%), respectively. On day 14, the percentage release of antibiotics (V_H and T_S) in FP from the control beads was 89.3% and 18% (undetected thereafter) and from the α-CSBG beads was 58.6% and 13.57%, respectively. On day 14, the percentage release of V_H and T_S in SBF from α-CSBG beads was 82% and 14.32%, respectively. The 14th day results showed that the elution of antibiotics in aqueous SBF was faster than in FP rich in organic matters, and PLGA coating had a considerable impact on suppression of release concentration and prolongation of the release period. The anticoagulant (CPDA1) containing plasma was clotted against the α-CSBG beads (Fig. S8).

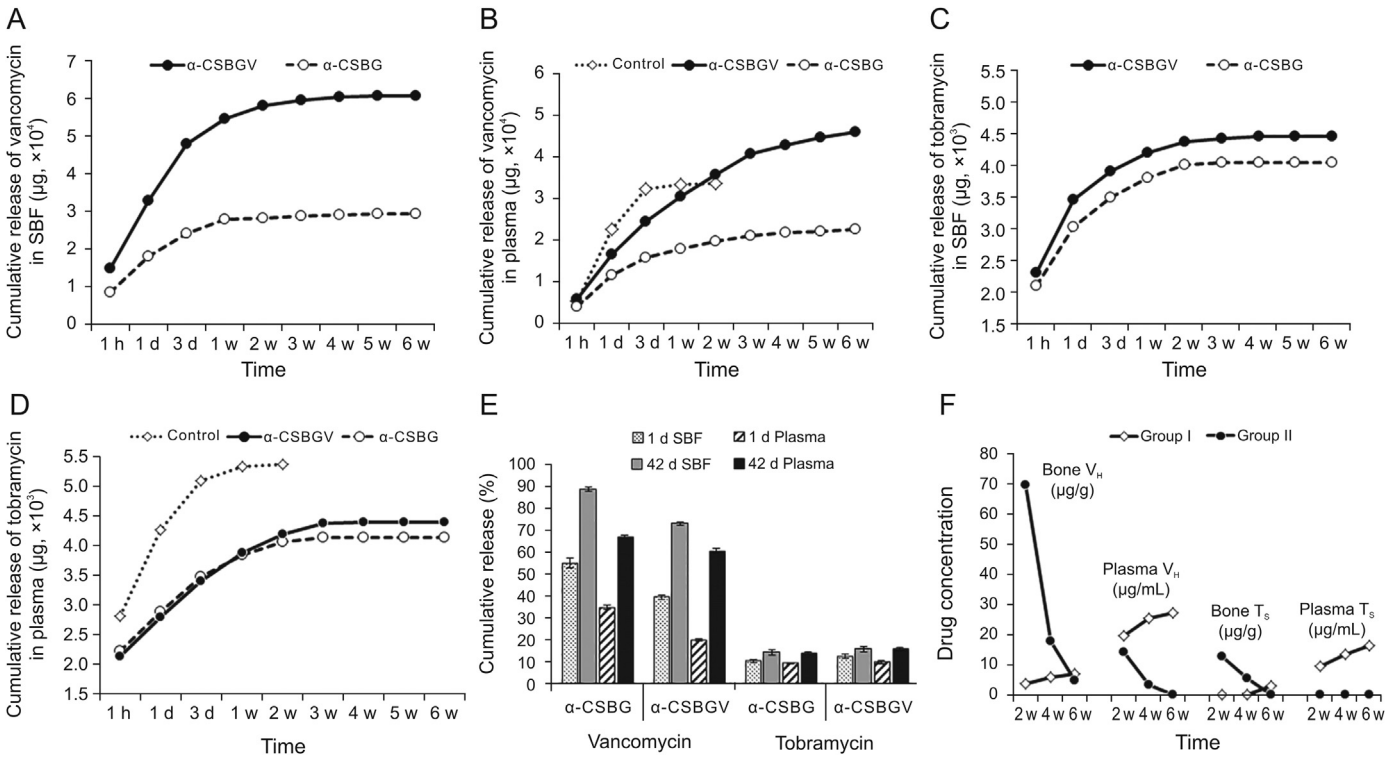

Fig. 5. Cumulative elution of (A and B) V_H and (C and D) T_S, (E) percent release at day 1 and day 42 from different beads in SBF and plasma, and (F) antibiotics (V_H and T_S) concentrations in plasma and bone for Group I and Group II animals.

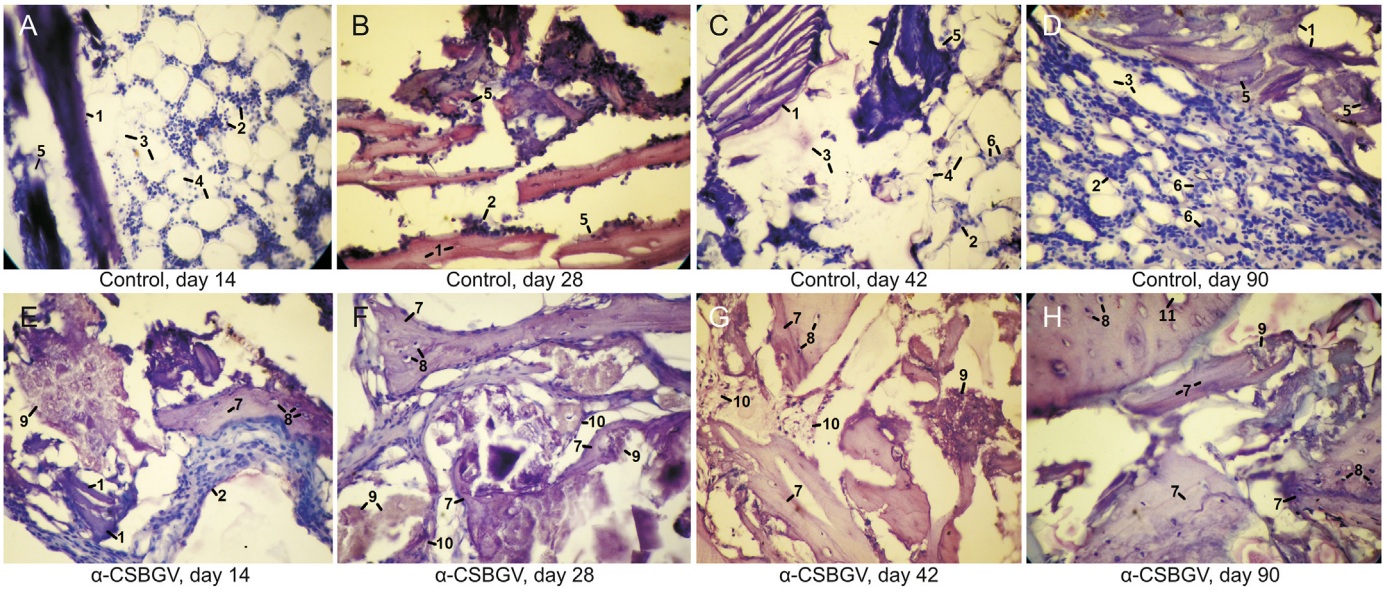

Fig. 6. Histological images of post-treated osteomyelitis defects show (A–D) poor recovery for Group I (control), and (E–H) adequate healing of sepsis and early bone regeneration with slow-resorptive cement over time for Group II (α-CSBGV). (1) Necrosed bone; (2) chronic inflammatory cells; (3) marrow exudate; (4) marrow degeneration; (5) resorbing dead bone; (6) giant cell; (7) osteoid; (8) osteoblasts; (9) osteoid-cement fusion; (10) proliferation of fibro-mesenchyme; (11) developing Haversian canal (magnification ×400).

3.2.4. *In vitro degradability and pH change*

The degradation (%) of α/β-CSH composites in SBF and FP and the changes in pH of SBF at 6 weeks for α-CSBG beads are shown in Figs. 3F and E. The degradation rate of bead surfaces was increased after 7 days of immersion. The pH value for α-CSBG beads gradually moved upward even when there were acidic antibiotics in the medium.

3.2.5. *In vitro bioactivity and cytocompatibility test*

The deposition of spherical calcium phosphate (apatite) precipitates throughout the α-CSBG surface was confirmed by FTIR and SEM-EDX analysis (Figs. 3G and S9). Fig. 3H shows MC3T3 cell proliferation in percentage on α-CSBG beads compared to α-CSH beads after 1, 3, and 7 days of culture, respectively. The proliferation

Fig. 7. Lateral skiagrams of tibia for (A–D) Group I, and (E–H) Group II with time. Arrow indicates resorbing cement and arrow head for bone fill in osteotomy hole. d: days; Gr.: group.

of MC3T3 cells cultured on the α-CSBG beads was markedly higher than that on α-CSH for the entire period. The results substantiated that the α-CSBG bead had superior biocompatibility. In SEM images, the living cells seemed to be more in number on the α-CSBG beads than on α-CSH beads at every study point but slightly decreased over both beads on day 7 than on day 3 (Fig. S10), which corroborated with MTT assay results.

3.2.6. Microbiological examination

Gram-positive strains (*S. aureus*) were observed in pus and marrow samples for every mammal after stage 1 surgery and for all Group I samples after stage 2. The microbial proliferation was identified with 2 Group II samples at 14 days p.i. and no growth detected thereafter.

3.2.7. Histopathological examination

The HP sections for all bone samples after the first surgery and Group I sections after the second (stage 2) surgery were matched with the typical features of chronic osteomyelitis (Figs. S11, 6A–D) including hypereosinophilic dead bone and osteocytes, perivascular chronic inflammatory cells, exudates, and bloated marrow parenchyma filled with numerous chronic inflammatory cells (mononuclear/giant cells). However, the degenerative/inflammatory changes were intensified after withdrawal of antibiotics on 90th day sections for Group I. The HP sections up to 42 days for Group II illustrated (Figs. 6E–G) progressive reduction of osteomyelitic changes in terms of mild chronic infiltrates in marrow, proliferation of vascular mesenchyme around the cement particles, formation of osteoid from developing osteoblasts, and resorption at

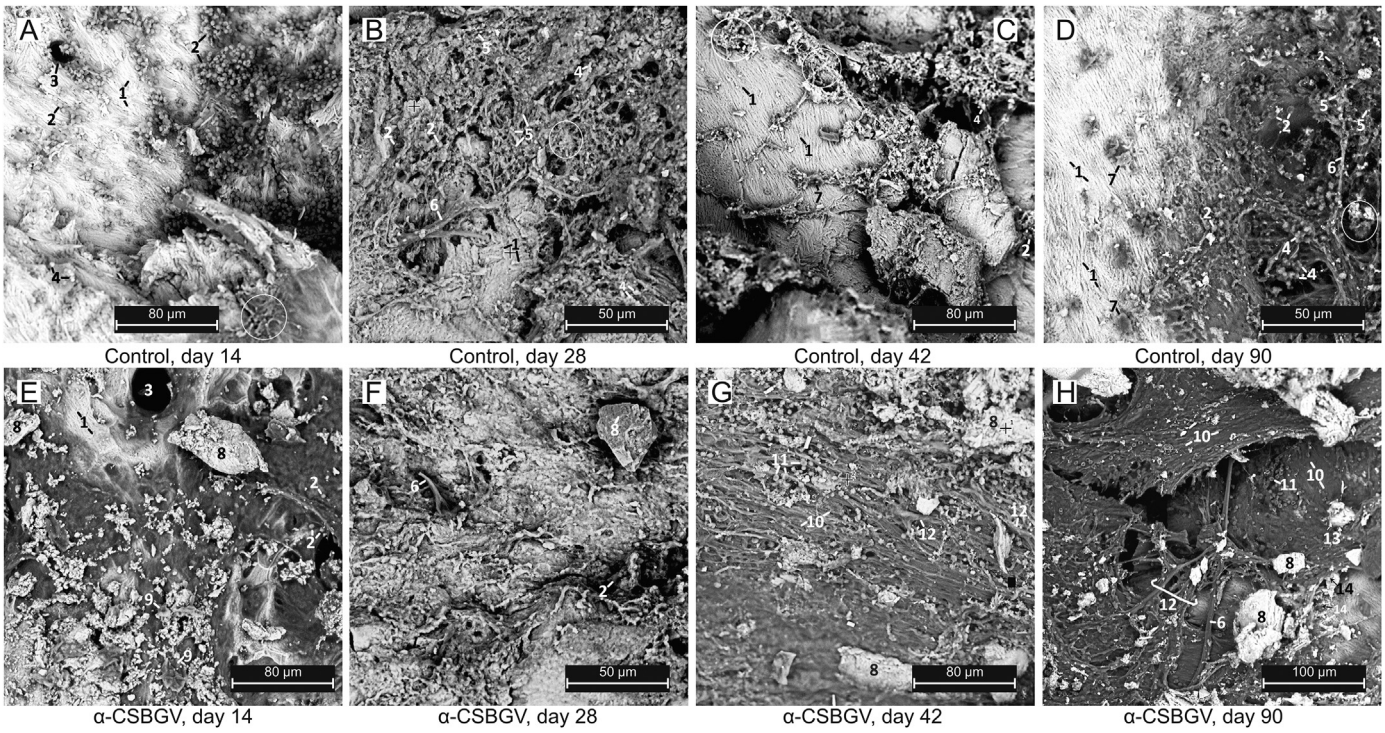

Fig. 8. Scanning electron micrographs of bone defects for (A–D) Group I (control), and (E–H) Group II (α-CSBGV) at specified time. (1) Uncalcified collagen of bone; (2) chronic infiltrates; (3) Haversian canal; (4) bacteria, (circle) exudate; (5) degenerated marrow; (6) blood vessels; (7) osteoclast-like cells; (8) cement materials; (9) osteoblasts; (10) mineralized osteoids; (11) red blood cells; (12) fibro-vascular proliferation; osteoid deposition over (13) cement, and (14) dead bone.

the margin of dead bone and cements. After 42 days, the Group II sections showed absence of chronic infiltrates and septic features along with distinct reparative features including fusion of cement materials with the callus, developing Haversian canals, and bone remodeling in few areas (Fig. 6H). Thus, the total HP score for Groups I and II was 45.89 ± 1.36 and 20.33 ± 1.32, respectively (Tables 4 and S6).

3.2.8. Radiographic observation

The development of chronic osteomyelitis in the radiographs of all mammals was witnessed by prominent sclerotic (radiodense) changes of endosteal trabeculae, mild periosteal thickening, and radiolucent (osteolysis) irregular margin around the osteotomy hole. Both the sclerotic and lytic changes were suggestive of osteomyelitis (Fig. S11). The gradual sclerosis of medullary bone along with blurred trabecular pattern around the cortical hole was evident in the radiographs for Group I animals throughout the study period (Figs. 7A–D). The radiographs for Group II showed radiodense non-resorbed cement beads close to the partially obliterated holes and revival of trabecular details in proximal metaphysis up to 28 days p.i.. At successive intervals, radiographs showed reestablishment of medullary radiolucency, disappearance of cement beads, lack of resorptive changes, and total disappearance of osteotomy holes (Figs. 7E–H). These observations demonstrated that the bone defects had undergone progressive healing and remodeling.

3.2.9. In vivo drug concentration

In every study point, drug level in plasma was notably lower than that in bone for Group II, whereas the differences were reversed for Group I animals (Fig. 5F and Table S7). The accumulation of drugs in plasma and sub-therapeutic level in bone were observed after parenteral therapy.

3.2.10. SEM of endosteal bone

The SEM micrographs of bone defects for all groups are shown in Figs. 8 and S11. The microstructures of bones after 30 days of stage 1 surgery and the Group I samples for entire study period demonstrated nearly similar features including discrete presence of decalcified collagen fibres in mature bone tissue and existence of bacteria, chronic infiltrates, and fibro-purulent contents within Haversian canal, degenerated fatty marrow, and on the bone surface. In the photomicrographs of Group II animals, chronic infiltrates containing fibro-vascular tissues and disorganized (immature) callus, osteoblasts, and entangling of residual cements in the bone tissue were observed up to 42 days p.i.. However, organized mature bone developed from osteoblasts and partially encased cement materials in the bone matrix on 90 days p.i., indicating mineralization process continued at various sites. The total SEM scores for Groups I and II were 47.33 ± 1.22 and 21.56 ± 1.51, respectively (Tables 4 and S8). It indicated superior efficacy of α-CSBGV in treating bone infection as the HP score than parenteral therapy.

4. Discussion

The present report discloses a new, injectable, antibiotics-eluting α–CSH–BG based composite bone cement for treating chronic osteomyelitis. This study also evaluated the salient properties (mechanical strength, biocompatibility, bioactivity, resorbability, and drug release kinetics) of the cement by examining laboratory findings in detail. Finally, the study compared the repair potential of the cement with respect to systemic antibiotic therapy in septic tibia of rabbits for 90 days.

The XRD and FTIR spectra revealed the lack of phase impurities in α-CSH and BG powders (Figs. 1 and 2). The oxide families of BG ceramics had a propensity to form amorphous sodium calcium silicate as the main phase in all the samples detected by XRD [5,14].

Silica content of the BG ceramics (43.72%) was safe for osteoblastic stimulation and bioactivity [22]. Although these ceramics allowed contact osteogenesis, high ions and drugs release due to faster dissolution of the CSD matrix, and low chemical durability due to rapid degradation of amorphous BG would undesirably affect the bone repair [23]. This limitation was partially negated by adjusting the sintering temperature and by encapsulating the drug loaded BG globules with the layers of PLGA and α-CSH. The DSC and SEM studies recognized the development of hard, non-porous α-CSH crystals. The α-CSH was used as a binder of BG particles. It could limit the rate of drug elution and enhance the mechanical property. Furthermore, it allowed the mixing of additive in the binder matrix with an insignificant alteration of the setting time and mechanical strength of the cement.

The BG granules showed uneven distribution of pores (Fig. 4), which might be due to unequal shrinkage of pores and fusion of glass grains during sintering or attributable to collapse of pores upon crushing of BG discs. When sintered above 710 °C, micropores were almost lost whereas inadequate granule structures were obtained below 670 °C. Hence, sintering temperature was optimized to 690 °C for BG discs, which was quite lower than the reported data [24]. In addition, crushing pressure should have profound effect on pore volume deterioration that was noticed when porosity of the scaffold and granules was compared (Table 3). The distribution of open pores and their interconnection in BG granules were found to be favourable for sufficient loading and sustainable release (micro/mesopore) of drugs and bone ingrowth (macropore). The loading of antibiotics into the BG granules was adequate, which might be due to good pore characteristics and/or the high affinity of organic drug molecules for the amorphous BG as well as high negative surface charge of the BG. Some drug moieties could bind on the surface of the glass by secondary bonding and the other fraction inside the pore channels that might be responsible for satisfactory drug adsorption (thick coat) [25]. The highly negative zeta potential of BG at pH 4.5–8.4 was another factor liable for strong electrostatic interaction of BG with cationic drug molecules (i.e., amide groups of T_S) within the stern layer as evidenced from SEM micrographs (Fig. 3). The setting time and mechanical strength are the two important properties of bone cement [15]. In α-CSH beads, the interlocking of needle-like CSD crystals contributes towards its compressive strength. The hydrophobic film (PLGA) between antibiotic loaded BG granules and binder (CSH) could reduce the retarding effect of drugs on the hydration reaction of cement. However, PLGA coating did not allow α-CSH particles to adapt well with the irregularities of BG surfaces during setting and prevent proper interlocking, resulting in decrease of strength of the cement. It was found that the addition of BG granules with α-CSH further shortened the setting time of pure α-CSH (IT: 7 min at 27 °C). The alkali ions dissolved out from BG into the slurry might be liable for faster setting of α-CSBG pellets. Other factors including optimum l:p ratio, short mixing time (30 s) to restrict additive dissolution and temperature of mixing kit had significant impacts on setting time and hardness of the cement [26]. This self-setting cement evolved low exothermic heat (<37 °C); hence, it causes no harm to the biological tissues. Practically, the incorporation of porous granules and the additive V_H (retarder) decreased the compression strength of the cement and rated the cement unsuitable for high load bearing application. However, the results showed that the average compressive failure load of the α-CSBG cement (11–18 MPa) was marginally higher than the reported tensile and compressive load of cancellous bone (2–16 MPa) [27]. Hence, the additive-free cement can be safely used in the semi load bearing applications. The injectability of cement usually correlates with the needle gauge, l:p ratio, and the cohesiveness and hardening rate of the paste [28]. Although the α-CSBG cement had several limitations including uneven flowability, poor cohesiveness, and slow setting in hydrophilic tissue sites, but it would be useful in remote areas of bone for its resorptive characteristic. The β-CSBG cement was not opted for animal studies because of low workability and strength, and high open porosity that could elute the antibiotics rapidly.

The plasma has been selected as an elution medium because it is the real body fluid that reflects free drug level in vivo for the cement beads. The aqueous SBF could diffuse freely into the pores and it had no proteinous molecules to bind antibiotics; hence, greater burst release was observed in SBF compared to plasma (Fig. 5). The interaction of FP containing platelets with the Ca^{2+} ions of the cement possibly worked for the activation of platelets and eventually coagulation of FP in drug elution study. After implantation into the surgical defects, a thick clot would form around the cement beads that might serve as the outermost barrier against drug elution other than pores, PLGA, and CSD matrix. The activated platelets could also secrete growth factors essential for wound repair. As the clot was liquified after gentle shaking, it did not adversely affect the release study. In addition, the plot for FP samples revealed a more sustainable mode of drugs release than SBF samples and absence of accessory humps adjacent to drug peak in HPLC. It indicated that FP would be a more authentic immersion medium than SBF to assess the drug release profile. The α-CSBG beads showed initial burst of antibiotics essential for reduction of large bacterial load; following that a sustainable mode of delivery to prevent disease recurrence and to afford time for immune cell growth against infection [29]. The faster release of antibiotics from the uncoated control pellets than α-CSBG indicated that PLGA barrier could substantially block the 'initial burst' and prolong the elution period of drugs from the α-CSBG beads [30,31]. It was expected that the antibiotics were eluted initially from the matrix and uncoated areas of the granules via diffusion. Subsequently, the hydrolyzed PLGA molecules were swollen inside the pore channels and permitted slow passage of drugs and metabolites via semi-porous network. The elution of V_H additive enhanced the release of both antibiotics by opening up the porous tunnels in the matrix, via which liquid could get access to the drugs trapped in the PLGA covered granules. Although tiny molecules of T_S (weight-average molecular weight (MW): 467.5 g/mol) would dissolute faster than V_H (MW: 1485.7 g/mol), the amount (<16%) and rate of T_S elution from the beads in both media were substantially lesser than those of the larger V_H molecules (>80%), surely due to disparity in adsorbed quantities and the additive usage. The elution of T_S was less affected with the alteration of medium because it was present only as a PLGA encapsulated form in the beads. Moreover, the chelation between oxide family of BG and T_S [22] and deeper entry of tiny T_S particles into the microporous core of BG granules could be accountable for low release. These barrier mechanisms would supervise the release kinetics both physically by blocking the route and chemically by slow dissociation of PLGA-drug-BG (oxide) chelates [32,33]. Furthermore, differences in the quantification methods of the antibiotics (bio-assay versus HPLC) may not be disregarded. The α-CSBG beads showed moderate degrading tendency in either immersion medium. It might be due to weak interlocking of CSD crystals with PLGA surfaces or derived from the alteration of bond strength between CSD and BG because of the low chemical stability (i.e., ionic exchange) of BG in the immersion medium. This was another reason for rapid release of high amounts of V_H from α-CSBGV beads [14,18]. The α-CSBG is completely biodegradable in nature; hence, the entire incorporated antibiotics would be released within the surgical site [3]. Furthermore, the V_H concentrations released from the composites (except control) were much lower than the published toxic levels (>2000 μg/mL) after day 1, thus emphasizing the potential role of degradable composite cement as a local drug carrier [34]. The surface degradation and

Table 4
Intra-group (paired *t*-test) and inter-group (independent *t*-test) analyses on the basis of estimated histopathology (HP) and scanning electron microscopy (SEM) scores of cellular events for the animal groups over time (mean ± SD).

Study interval	HP		IS *t*-test	SEM		IS *t*-test
	Group I	Group II		Group I	Group II	
14 days	11.67 ± 1.0†	10.1 ± 0.78	t=3.677*	12.2 ± 1.09†,¶	9.44 ± 0.73	t=6.35*
28 days	11.1 ± 0.78†,¶	6.67 ± 1.2	t=9.067*	11.2 ± 0.67$^{\dagger,\#}$	6.89 ± 0.93	t=11.377*
42 days	10.2 ± 0.83¶	2.1 ± 0.93†	t=19.51*	10.67 ± 0.7$^{\#}$	3.33 ± 0.5	t=25.403*
90 days	12.89 ± 0.78	1.3 ± 0.71†	t=32.888*	13.2 ± 0.67¶	1.89 ± 0.6	t=37.882*
Gross score	45.89 ± 1.36	20.33 ± 1.32	t=40.345*	47.33 ± 1.22	21.56 ± 1.51	t=39.788*

Same superscripts (†, ¶, and $^{\#}$) indicate statistically insignificant difference (P>0.05) in a group with time. *Significant inter-group relation at specific time interval (P<0.05); SD: standard deviation; IS: independent sample.

high cations content (bacteriostatic) of α-CSBG would deter the surface adhesion of bacteria [35]. Apart from lowering the resorbability of CSD, the BG granules in the system increased the osteogenic potential of the construct by triggering rapid osteoblasts adhesion on its negatively charged surfaces [4,7,36]. In our report, the beads were biodegraded steadily but concurrently with drug elution. Therefore, diffusion dominated elution kinetics was observed in the beginning and later, and concurrent degradation associated release (PLGA and CSH) with the diffusion from the pores was evident [37]. The prolonged elution profiles of the antibiotics from the cement beads violated the simple mathematical models (e.g., Peppas model) of release kinetics. It was because either both elutes adopted multiple release kinetics (diffusion/degradation) or other factors (polymer-drug synergy, multi-barrier, heterogeneous mixing, and drug solubility) could start leading the elution mechanisms after a certain period [38]. The cationic BG granules would drop the dissolution of free drug bases or could neutralize the acidic metabolites of PLGA polymer; these facts also explained why the release kinetics did not follow the simple models [32]. The gradual pH rise of the cement containing SBF solution was primarily due to the influence of BG (pH 11–12.5) granules [18]. Several literatures reported multiple benefits of alkali ions (i.e., Na^{+}, Ca^{2+}, and SiO_2) leaching from BG granules into the tissue sites including interference with biofilm growth [35], antimicrobial effect against *S. aureus* [23] and pivotal role in angiogenesis and bone healing [7,23]. Above pH 7.4, osteoclast cells lose their bone resorbing ability, whereas alkaline phosphatase activity significantly increases in osteoblasts [39]. Hence, the insertion of composite cement in the bone sepsis (pH<6.0) could possibly shift the pH of the tissue toward alkaline and would serve the aforesaid benefits along with the local release of antimicrobials. Furthermore, the α-CSBG beads offered a more suitable environment for cell proliferation in the culture study than α-CSH, which might be due to the stimulatory effects of BG on MC3T3s and local pH variation. The gradual rise in pH after soaking of the composite in SBF indicated that the released cations from the BG could surpass the acidic pH of V_H and SBF. Since acidic ambience restricts cell division [40], the neutral α-CSH beads showed less cytocompatibility than the basic α-CSBG beads. Moreover, the proliferation of precursor cells could be triggered by the dissolution byproducts of BG [41] and less degradable surface of the composite. After 7 days, the quantities of cultivated cells on both the specimens were decreased but the concentration of cells on the α-CSBG beads was invariably higher (P<0.05) than those observed on the α-CSH samples. The increased rate of surface degradation of both the beads on 7 days might have resulted in some loosening of attached cells which were washed out during processing of the samples. It could be the major cause of decreased cell proliferation on 7 days of culture than on 3 days. The increased cell concentration on α-CSBG beads strongly indicates that the addition of BG to CSH could have a positive impact on osteoblasts proliferation [7]. Hence, the α-CSBG possessed superior in vitro cytocompatibility and bioactivity, and exhibited huge capability for osseous reconstruction. Eventually, we selected the α-CSH based ceramic bone cements for the animal experimentation due to its aforesaid beneficial properties in research lab.

Histological examination is the most reliable investigation for diagnosis as well as assessment of the therapeutic responses of different remedies in chronic osteomyelitis because it renders thorough understanding about the cell/tissue changes in infection and subsequent healing phases [42]. The MT is the second choice because it can occasionally give false negative outcomes. The MT could not identify the pathogenic involvement in two bone defects. But they were recognized as bone infection with HPE, suggesting MRSA bone infection was developed satisfactorily in every rabbit that was again supported by the osteolytic and sclerotic changes in X-ray images. Both the HP findings and the comparative values of HP scores showed rapid and satisfactory resolution of bone infection with Group II animals (Fig. 6 and Table 4). This might be attributed to excellent pharmacokinetics of α-CSBGV beads as evident from drug elusion study in plasma. After significant decline in antibiotic release from 42 days onwards, the cement became resorbed slowly to allot room for proliferation of fibro-mesenchymal tissues and eventually trapped into the new osteoid as evident in the HP images. Accordingly, α-CSBG cement could be regarded as a composite with high bioactivity and the degradation rate of the cement was almost equivalent to the rate of ossification, thus eliminating the necessity of second surgery for cement removal. The infective features of bone sepsis in Group I animals were observed at every study point, suggesting minimal effectiveness of systemic antibiotics in resolving infection of long bones. The radiodensity of cement revealed a beneficial property for locating its position in vivo after implantation and successive phases of bone healing. The almost disappearance of cortical boreholes in the X-ray images with Group II animals indicated that the repair and remodeling of cortical bone could be associated with early suppression of bone sepsis and immense osteogenic capacity of the α-CSBG cement (Fig. 7).

In support of the in vitro elution study, it could be stated that the pharmacokinetics of the beads effectively maintained the curative concentration of antibiotics many times greater than the MIC for MRSA (MIC of T_S: <2.0 μg/mL, V_H: <1.0 μg/mL) at the tissue sites for 5–6 weeks to eradicate the bone sepsis [1]. The ineffectiveness of parenteral antibacterial drugs in Group I was attributed to inaccessibility of the drugs in achieving sufficient concentration at poorly perfused necrotic bones and due to the presence of functional blood-bone marrow barrier [43]. The level of both antibiotics for Group I was just above the MIC or undetectable in bone and close to the toxic level in plasma that was ineffective in inhibiting biofilm-enclosed bacterial colonies but could raise the risk of drug toxicity. Similar interference was also liable for limited exchange of drugs from bone to the blood in Group II, which gave adequate protection to the rabbits from high local concentration of antibiotics with no major side effects. Large variation in drugs level at plasma and bone for Group II would support the aforesaid statements about safety of bone cement [12].

The micrograph of the treated defects and SEM scores for both the groups were in agreement with the histological features of bone (Fig. 8 and Table 4). In SEM micrographs for Group II, the early and mature osteogenesis encircling the dead bone and cement surfaces was evident. Almost parallel bone-friendly characteristic of the bioactive ceramic composites was reported earlier [7,15]. Adequate healing response in terms of reparative changes, neovascularisation, and active growth of osteoblasts was also observed with Group II. The simple method of antibiotics loading at RT would possibly neither degrade nor affect the antibacterial activity of the antibiotics.

Recently, several advanced technologies, such as engineered 3-dimensional (3D) scaffolds [44], electroactive tissue engineering scaffolds [45], electrospun polymer micro/nanofibres [46] and antibacterial hydrogels [47], have been investigated as platforms for guided delivery of drugs (antibiotics, anticancer drugs, and growth factors) in the bone defects. The improved biocompatibility, biodegradability, high surface area, complex pore structures, and efficient drug release profiles are all important advantages that can serve the newer scaffolds. However, the moldability and strength of these biomaterials are not adequate for stress bearing application. Among these newer biomaterials, the electroactive conducting polymer (polyaniline) scaffolds and polymer based antibacterial hydrogels loaded with inorganic metallic ions or antibiotics appear to be the promising candidates for remission of bone sepsis due to their stimulated switch on-off release property. Owing to the matched useful properties (biocompatibility, porosity, strength etc.), further work is required to investigate the suitability of α-CSBG cement as an engineered 3D scaffold to achieve the best therapeutic effect in various osseous abnormalities.

There were some limitations with the present study design too. The efficacy of the α-CSBG cements could be best judged if another group treated with local and short-term parenteral antibiotics would be included. The influence of time of mixing of additive in cement on setting time and plasma level of cations (Ca^{2+} and Na^{+}) after implantation of α-CSBG beads was not assessed. Moreover, accurate assessment of the rheometrical behavior of the self-setting α-CSBG paste would not be possible due to the on-going hardening reaction of the cement mix.

5. Conclusion

An innovative drug-carrying biodegradable composite bone cement formulation has been developed successfully by mixing of PLGA coated bioactive glass granules loaded with antibiotics, the binder α-CSH and an optional powdered antibiotic. The results of laboratory tests reveal that the constituents of the composite cement are pure and biocompatible and have excellent physico-chemical properties suitable for the production of drug-eluting bone cement and its implantation in tissues. The PLGA coating and adjusted physico-mechanical properties of the cement (setting time, strength, injectability, and biodegradation), and further improved the working time, applicability, and the control over drug elution profile for sufficient duration effectively to combat chronic osteomyelitis. Besides, the enhanced cytocompatibility and tailored degradability of the cement facilitate osteoconduction as well as prevent bacterial adhesion on the degrading bead surface. Furthermore, the estimated level of antibiotics showed that the drug release was higher than MIC against *S. aureus* for the entire study period with no systemic toxicity. The results of animal study also established the superiority of Group II over Group I in terms of eradication of bone sepsis and osteogenesis. In addition to multi-layered barrier (pores, PLGA, and binder) effect on drug release, coagulation in contact with the composite struts is thought to restrict further drug release and hasten bone healing via release of growth factors from the activated platelets. Therefore, we conclude that α-CSBG bone cement is found to be the worthy drug carrier for antibiotics, which rule out the second surgery unlike PMMA cement. It is also feasible to develop multipurpose cement for various bone diseases such as osteoporosis by changing only the bimolecular component. Further research to improve the strength of α-CSH is highly appreciated for heavy stress bearing applications.

CRediT author statement

Surajit Mistry: Conceptualization, Methodology and Investigation; **Subhasish Burman:** Data collection and Assists surgeon; **Subhasis Roy:** Principal surgeon, Animal care and Analyze investigation report; **Nilendu Jyoti Maitra:** Analysis and Interpretation of results; **Rajiv Roy:** Methodology, Writing - Original draft preparation; **Abhijit Chanda:** Supervision and Data curation.

Declaration of competing interest

The authors declare that there are no conflicts of interest.

Appendix A. Supplementary data

Supplementary data to this article can be found online at https://doi.org/10.1016/j.jpha.2021.02.005.

References

[1] Z. Xie, X. Liu, W. Jia, et al., Treatment of osteomyelitis and repair of bone defect by degradable bioactive borate glass releasing vancomycin, J. Contr. Release 139 (2009) 118–126.
[2] T.A.G. van Vugt, J.J. Arts, J.A.P. Geurts, Antibiotic-loaded polymethylmethacrylate beads and spacers in treatment of orthopedic infections and the role of biofilm formation, Front. Microbiol. 10 (2019), 1626.
[3] W.J. Habraken, J.G. Wolke, J.A. Jansen, Ceramics composites as and scaffolds for drug delivery in tissue engineering, Adv. Drug Deliv. Rev. 59 (2007) 234–248.
[4] P.-Y. Hsu, H.-C. Kuo, W.-H. Tuan, et al., Manipulation of the degradation behavior of calcium sulfate by the addition of bioglass, Prog. Biomater. 8 (2019) 115–125.
[5] Q.Z. Chen, I.D. Thompson, A.R. Boccaccini, 45S5 Bioglass-derived glass ceramic scaffolds for bone tissue engineering, Biomaterials 27 (2006) 2414–2425.
[6] X. Zhang, W. Jia, Y. Gu, et al., Teicoplanin-loaded borate bioactive glass implants for treating chronic bone infection in a rabbit tibia osteomyelitis model, Biomaterials 31 (2010) 5865–5874.
[7] Y. Zheng, C. Xiong, D. Zhang, et al., In vitro bioactivity evaluation of α-calcium sulphate hemihydrate and bioactive glass composites for their potential use in bone regeneration, Bull. Mater. Sci. 41 (2018), 59.
[8] B.D. Ulery, L.S. Nair, C.T. Laurencin, Biomedical applications of biodegradable polymers, J. Polym. Sci. B Polym. Phys. 49 (2011) 832–864.
[9] L. Zhao, C. Wu, K. Lin, et al., The effect of poly(lactic-co-glycolic acid) (PLGA) coating on the mechanical, biodegradable, bioactive properties and drug release of porous calcium silicate scaffolds, Biomed. Mater. Eng. 22 (2012) 289–300.
[10] G. Giavaresi, E. Bertazzoni Minelli, M. Sartori, et al., Microbiological and pharmacological tests on new antibiotic-loaded PMMA-based composites for the treatment of osteomyelitis, J. Orthop. Res. 30 (2012) 348–355.
[11] J. Slane, B. Gietman, M. Squire, Antibiotic elution from acrylic bone cement loaded with high doses of tobramycin and vancomycin, J. Orthop. Res. 36 (2018) 1078–1085.
[12] R.P. Howlin, M.J. Brayford, J.S. Webb, et al., Antibiotic-loaded synthetic calcium sulfate beads for prevention of bacterial colonization and biofilm formation in periprosthetic infections, Antimicrob. Agents Chemother. 59 (2015) 111–120.
[13] H. Ding, C.-J. Zhao, X. Cui, et al., A novel injectable borate bioactive glass cement as an antibiotic delivery vehicle for treating osteomyelitis, PLoS One 9 (2014), e85472.
[14] S.K. Ghosh, S.K. Nandi, B. Kundu, et al., In vivo response of porous hydroxyapatite and beta-tricalcium phosphate prepared by aqueous solution combustion method and comparison with bioglass scaffolds, J. Biomed. Mater. Res. B Appl. Biomater. 86 (2008) 217–227.
[15] W. Zhou, Y. Xue, X. Ji, et al., A novel injectable and degradable calcium phosphate/calcium sulfate bone cement, Afr. J. Biotechnol. 10 (2011) 19449–19457.
[16] G.O.K. Loh, K.B. Liew, K.K. Peh, et al., Simple high performance liquid chromatography method for determination of norfloxacin in plasma and

application in bioequivalence study, Int. J. Pharm. Pharmaceut. Sci. 4 (2012) 247–251.
[17] M. Balouiri, M. Sadiki, S.K. Ibnsouda, Methods for *in vitro* evaluating antimicrobial activity: a review, J. Pharm. Anal. 6 (2016) 71–79.
[18] C. Soundrapandian, D. Basu, B. Sa, et al., Local drug delivery system for the treatment of osteomyelitis: in vitro evaluation, Drug Dev. Ind. Pharm. 37 (2011) 538–546.
[19] L. Fu, W. Xia, T. Mellgren, et al., Preparation of high percentage α-calcium sulfate hemihydrate via a hydrothermal method, J. Biomaterials Nanobiotechnol. 8 (2017) 36–49.
[20] V. Leškevičienė, α-Hemihydrate gypsum from flue gas desulphurization gypsum, Mater. Sci-Medzg. 19 (2013) 197–202.
[21] X.-Q. Wu, Z.-B. Wu, Modification of FGD gypsum in hydrothermal mixed salt solution, J. Environ. Sci. (China) 18 (2006) 170–175.
[22] L.L. Hench, Bioceramics: from concept to clinic, J. Am. Ceram. Soc. 74 (1991) 1487–1510.
[23] S. Zahid, A.T. Shah, A. Jamal, et al., Biological behavior of bioactive glasses and their composites, RSC Adv. 6 (2016) 70197–70214.
[24] D. Bellucci, A. Sola, V. Cannillo, et al., Low temperature sintering of innovative bioactive glasses, J. Am. Ceram. Soc. 95 (2012) 1313–1319.
[25] Y. Zhu, S. Kaskel, Comparison of the in vitro bioactivity and drug release property of mesoporous bioactive glasses (MBGs) and bioactive glasses (BGs) scaffolds, Microporous Mesoporous Mater. 118 (2009) 176–182.
[26] S.V. Dorozhkin, Self-setting calcium orthophosphate formulations, J. Funct. Biomater. 4 (2013) 209–311.
[27] L.-C. Gerhardt, A.R. Boccaccini, Bioactive glass and glass-ceramic scaffolds for bone tissue engineering, Materials 3 (2010) 3867–3910.
[28] A.-M. Yousefi, A review of calcium phosphate cements and acrylic bone cements as injectable materials for bone repair and implant fixation, J. Appl. Biomater. Funct. Mater. 17 (2019), https://doi.org/10.1177/2280800019872594.
[29] M. Zilbermann, J.J. Elsner, Antibiotic-eluting medical devices for various applications, J. Contr. Release 130 (2008) 202–215.
[30] L. Du, S. Yang, W. Li, et al., Scaffold composed of porous vancomycin-loaded poly(lactide-co-glycolide) microspheres: a controlled-release drug delivery system with shape-memory effect, Mater. Sci. Eng. C Mater. Biol. Appl. 78 (2017) 1172–1178.
[31] Y.F. Zhao, S.C. Loo, Y.Z. Chen, et al., In situ SAXRD study of sol–gel induced well-ordered mesoporous bioglasses for drug delivery, J. Biomed. Mater. Res. A 85 (2008) 1032–1042.
[32] A.R. Boccaccini, V. Maquet, Bioresorbable and bioactive polymer/bioglass® composites with tailored pore structure for tissue engineering applications, Compos. Sci. Technol. 63 (2003) 2417–2429.
[33] H.-W. Kim, E.-J. Lee, I.-K. Jun, et al., Degradation and drug release of phosphate glass/polycaprolactone biological composites for hard-tissue regeneration, J. Biomed. Mater. Res. B Appl. Biomater. 75 (2005) 34–41.
[34] V. Antoci Jr., C.S. Adams, N.J. Hickok, et al., Antibiotics for local delivery systems cause skeletal cell toxicity in vitro, Clin. Orthop. Relat. Res. 462 (2007) 200–206.
[35] L. Drago, M. Toscano, M. Bottagisio, Recent evidence on bioactive glass antimicrobial and antibiofilm activity: a mini-review, Materials (Basel) 11 (2018), 326.
[36] C. Gauland, Managing lower-extremity osteomyelitis locally with surgical debridement and synthetic calcium sulfate antibiotic tablets, Adv. Skin Wound Care 24 (2011) 515–523.
[37] U. Gbureck, E. Vorndran, J.E. Barralet, Modeling vancomycin release kinetics from microporous calcium phosphate ceramics comparing static and dynamic immersion conditions, Acta Biomater. 4 (2008) 1480–1486.
[38] Y. Fu, W.J. Kao, Drug release kinetics and transport mechanisms of non-degradable and degradable polymeric delivery systems, Expert Opin. Drug Deliv. 7 (2010) 429–444.
[39] T.R. Arnett, Extracellular pH regulates bone cell function, J. Nutr. 138 (2008) 415S–418S.
[40] Y. Shen, W. Liu, K. Lin, et al., Interfacial pH: a critical factor for osteoporotic bone regeneration, Langmuir 27 (2011) 2701–2708.
[41] Z. Huan, J. Chang, Self-setting properties and in vitro bioactivity of calcium sulfate hemihydrate-tricalcium silicate composite bone cements, Acta Biomater. 3 (2007) 952–960.
[42] M. Panteli, P.V. Giannoudis, Chronic osteomyelitis: what the surgeon needs to know, Effort Open Rev. 1 (2017) 128–135.
[43] R. Saikia, A.K. Goswami, H.K. Sharma, Drug delivery to brain and bone marrow: a review, Eur. J. Biomed. Pharmaceut. Sci. 3 (2016) 604–616.
[44] T. Zhu, Y. Cui, M. Zhang, et al., Engineered three-dimensional scaffolds for enhanced bone regeneration in osteonecrosis, Bioact. Mater. 5 (2020) 584–601.
[45] L. Cui, J. Zhang, J. Zou, et al., Electroactive composite scaffold with locally expressed osteoinductive factor for synergistic bone repair upon electrical stimulation, Biomaterials 230 (2020), 119617.
[46] X. Feng, J. Li, X. Zhang, et al., Electrospun polymer micro/nanofibers as pharmaceutical repositories for healthcare, J. Contr. Release 302 (2019) 19–41.
[47] S. Li, S. Dong, W. Xu, et al., Antibacterial hydrogels, Adv. Sci. 5 (2018), 1700527.